

# Acetyl zingerone ameliorates osteoarthritis by inhibiting chondrocyte programmed cell death

XU CHEN<sup>1\*</sup>, JIE CHEN<sup>1\*</sup>, CHUNBAO MIAO<sup>2</sup>, GUANGRONG YIN<sup>1</sup>,  
ZHUANGZHUANG ZHANG<sup>1</sup>, RONGBIN SUN<sup>1\*\*</sup> and SU NI<sup>1\*\*</sup>

<sup>1</sup>Department of Orthopedics, The Affiliated Changzhou Second People's Hospital of Nanjing Medical University, Changzhou Second People's Hospital, Changzhou Medical Center, Changzhou, Jiangsu 213003;

<sup>2</sup>Jiangsu Key Laboratory of Advanced Catalytic Materials and Technology, Jiangsu Province Key Laboratory of Fine Petrochemical Engineering, School of Petrochemical Engineering, Changzhou University, Changzhou, Jiangsu 213164, P.R. China

Received May 12, 2023; Accepted August 16, 2023

DOI: 10.3892/mmr.2023.13089

**Abstract.** Osteoarthritis (OA) is a degenerative disease that ultimately leads to joint deformity. The pathogenesis of OA is believed to involve abnormal chondrocyte death, with ferroptosis serving a key role in chondrocyte damage. The present study investigated whether acetyl zingerone (AZ), a newly identified antioxidant derived from curcumin, can alleviate the progression of OA. To investigate this, the present study performed various experiments, including crystal violet staining, flow cytometry, immunofluorescence and western blot analysis. In addition, dual validation was performed using *in vivo* and *in vitro* experiments; a mouse OA model was constructed for the *in vivo* experiments, and chondrocytes were used for the *in vitro* experiments. Destabilization of the medial meniscus (DMM) surgery was performed to establish an OA model in mice and IL-1 $\beta$  was used to induce an OA model *in vitro*. The results indicated that AZ may promote chondrocyte viability and the expression of extracellular matrix components. Furthermore, AZ reduced the occurrence of ferroptosis by promoting the expression of glutathione peroxidase 4, inhibiting cartilage destruction and osteophyte formation, and alleviating damage to articular cartilage caused by DMM surgery. Mechanistically, the activation of nuclear factor erythroid 2-related factor 2 and heme oxygenase-1 may be responsible for the anti-ferroptosis effects of AZ

on chondrocytes. These findings indicated that AZ may be considered a promising candidate for OA therapy.

## Introduction

Osteoarthritis (OA) is a substantial global economic and familial burden (1). The epidemiology of OA is complex and multifaceted and includes a variety of genetic, biological, and biomechanical factors. Clinical manifestations of OA primarily include recurrent joint pain, limited mobility, and progressive joint deformity (2-4). As the hallmarks of OA, abnormal chondrocyte death, cartilage extracellular matrix (ECM) destruction and abnormal homeostasis are gaining more attention as therapeutic targets for cartilage regeneration (5,6). Moreover, during the progression of OA, the cartilage ECM undergoes substantial pathological alterations, which can act as promising biomarkers in identifying the pathological stages of OA (7). Evidence has suggested that chondrocytes undergo diverse forms of cell death, including necroptosis, apoptosis and ferroptosis, in OA (8,9). A recent study demonstrated that knockdown of the ferritin regulator NCOA4 can suppress IL-1 $\beta$ -induced ferroptosis and ECM degradation in chondrocytes (10). This indicates that ferroptosis acts on not only chondrocytes themselves but also on the chondrocyte ECM.

Ferroptosis, a form of programmed cell death involving iron and lipid peroxidation metabolism, is distinct from apoptosis and necrosis in terms of cell morphology, protein expression and genetic mechanisms (11-14). It has been reported that ferroptosis is widespread in chondrocytes in OA, and the role of glutathione peroxidase 4 (GPX4), a key regulator of ferroptosis, has also been extensively studied (15-17). Downregulation of GPX4 can increase the sensitivity of chondrocytes to oxidative stress and intensify degradation of the ECM through the MAPK/NF- $\kappa$ B pathway, thereby exacerbating the OA process (18). Additionally, osteophyte formation has been shown to be significantly increased in a mouse model of OA, and this effect was revealed to be further enhanced by the knockdown of GPX4 (18). Recently, several chemicals, such as curcumin and quercetin, have been reported to protect

**Correspondence to:** Dr Rongbin Sun or Dr Su Ni, Department of Orthopedics, The Affiliated Changzhou Second People's Hospital of Nanjing Medical University, Changzhou Second People's Hospital, Changzhou Medical Center, 68 Ge Hu Middle Road, Changzhou, Jiangsu 213003, P.R. China

E-mail: rongbin\_sun@sina.com

E-mail: vivian.nisu@gmail.com

\*\*\* Contributed equally

**Key words:** chronic pain, inflammation, arthritis, oxidative stress

chondrocytes from pathological ferroptosis and thus to ameliorate the progression of OA (19-21). Therefore, the development of ferroptosis inhibitors holds potential for augmenting the efficacy of existing treatment modalities and addressing the shortcomings of drug-based interventions.

Nuclear factor erythroid 2-related factor 2 (Nrf2) serves a crucial role in maintaining cellular homeostasis under oxidative stress conditions (22), as well as a key role in mediating iron/heme metabolism (23). Ferroptosis is triggered by the iron-dependent oxidation of polyunsaturated fatty acids, and Nrf2 specifically inhibits ferroptosis by reducing lipid peroxidation (24). Ferritin and iron transporters are controlled by Nrf2 (25,26). Numerous studies have shown that antioxidants affect ferroptosis via Nrf2 activation. For example, Guo *et al* (27) reported that deferoxamine alleviated OA by inhibiting chondrocyte ferroptosis and activating the Nrf2 pathway. Moreover, biochanin A can protect against iron overload associated with knee OA by regulating iron levels and the Nrf2/system  $x_c^-$ /GPX4 axis (19,28). Its pivotal role makes it an important candidate for mediating protective or deleterious effects through ferroptosis. Previous studies have also reported that heme oxygenase-1 (HO-1), a classic downstream antioxidant protein of Nrf2, is widely involved in ferroptosis (29,30). Furthermore, several lines of evidence have highlighted the role of HO-1 in the progression of OA, and its expression and activity are associated with cartilage growth, apoptosis, and ferroptosis (31-35). These results provide a potential treatment for OA in the form of a compound targeting the Nrf2/HO-1 pathway.

*Curcuma longa* L. is a traditional Chinese herb that is widely used in the treatment of rheumatoid arthritis, stroke, Alzheimer's disease, and even cancer; curcumin is the best studied active ingredient of *C. longa* due to its antioxidative and anti-inflammatory properties (36,37). However, its low solubility and low absorption in the human gut limit its application. Acetyl zingerone (AZ), a stable and more powerful derivative of curcumin, has been shown to protect skin cells from DNA damage (38), inhibit metalloproteinases (39), and stabilize other reducing agents to exert high-efficiency antioxidative effects and increase collagen levels (40). The main principle of the Fenton reaction is the addition of an  $H_2O_2$  oxidizing agent and a  $Fe^{2+}$  catalyst, both of which react under acidic conditions (generally pH <4) to produce hydroxyl radicals. Compared with curcumin, AZ has higher solubility, better photostability, and a much higher absorption rate, and AZ can inhibit the Fenton reaction (41). The latest research has shown that hyperoside, a flavonoid compound similar to AZ, exerts anti-OA effects through its anti-apoptosis and anti-inflammatory effects *in vitro* and *in vivo* (42); therefore, it was hypothesized that AZ would have a positive effect on OA. The present study aimed to investigate whether AZ can alleviate ferroptosis in OA by mediating Nrf2/HO-1 signaling; the data may provide new insights and targets for the treatment of OA.

## Materials and methods

**Reagents.** AZ was synthesized by Dr Miao's laboratory at Changzhou University (Changzhou, China). Recombinant rat IL-1 $\beta$  (cat. no. M21094) and ML385 (Nrf2 inhibitor) (cat. no. M8692) were purchased from Abmole Bioscience,

Inc. Ferrostatin-1 (Fer-1), a potent and selective ferroptosis inhibitor and the HO-1 inhibitor tin protoporphyrin IX (cat. no. 14325-05-4) were purchased from MedChemExpress. BeyoClick™ 5-ethynyl-2'-deoxyuridine (EdU)-488 Cell Proliferation Assay Kit (cat. no. C0071S), Cell Counting Kit-8 (CCK-8; cat. no. C0037), a reactive oxygen species (ROS) detection kit (cat. no. S0033), Calcein/PI Cell Viability/Cytotoxicity Assay Kit (cat. no. C2015M) and the Annexin V-FITC/PI Cell Apoptosis Detection kit (cat. no. C1062S) were purchased from Beyotime Institute of Biotechnology. Type II collagenase (cat. no. LS004176) was purchased from Worthington Biochemical Corporation. Super sensitive ECL luminescence substrate (cat. no. U10010A) was supplied by Yuyou Biotechnology Co., Ltd. The ATDC5 mouse chondrogenic cell line (cat. no. ZQ0938) was purchased from Shanghai Zhongqiao Xinzhou Biotechnology Co., Ltd.

**Nuclear magnetic resonance (NMR) experiments and analysis.** NMR spectra were run on a 500 MHz Bruker AVANCE DRX instrument using a broadband probe equipped with a z-gradient coil (Bruker). For NMR, a 600- $\mu$ g sample of AZ was run in standard 5-mm NMR tubes at 25°C. Pulse programs used were standard sequences taken from the Bruker XWINNMR pulse sequence library. NMR experiments were set up and processed generally using the parameters according to the manufacturer's protocol. The pulse programs selected for the 2D homonuclear chemical shift, heteronuclear multiple quantum coherence, and  $^1H$  detected heteronuclear multiple bond correlation experiments employed z-gradients for coherence pathway selection.  $^1H$  and  $^{13}C$  chemical shifts were calibrated relative to the solvents and tetramethyl silane. To determine the content of AZ in the sample, measurement analysis was performed. To calculate AZ content, the absorption peak area ( $A1/n1$ ) caused by a proton on AZ was compared with the absorption peak area ( $A2/n2$ ) caused by a proton on the sample, and the content of AZ was calculated according to the following formula. Relative percentage of the  $AZ = \{(A1/n1)/(A2/n2)\} \times 100$ .

**Isolation and culture of primary rat chondrocytes.** A total of 10 8-week-old male Sprague-Dawley rats (weight, 220 g) were purchased from Changzhou Cavens Experimental Animal Co., Ltd. and were maintained under the following conditions: 20-25°C, 50-60% humidity, free access to pure water and special feed, under a 12-h light/dark cycle. The rats were sacrificed within a week of purchase. Chondrocytes were isolated from the articular cartilage of 8-week-old male Sprague-Dawley rats. The present study was approved by the Jiangsu Science Standard Medical Testing Committee (approval no. IACUC22-0097), which is a regional committee that sets standards for scientific research in Jiangsu province. For the extraction of chondrocytes, rats were sacrificed the day after arrival by  $CO_2$  asphyxiation (fill rate, 60% chamber volume/min), and death was confirmed by observing a lack of respiration and faded eye color (42,43). The method of sacrifice used is able to fulfill the objective of rapid unconsciousness with minimal distress to the animals (44). After the rats were sacrificed, they were sterilized with 75% ethanol and iodophor, and the cartilage tissues of the rat knee joints were collected in a biological safety cabinet hood and placed

into PBS (cat. no. P1010-2L; Beijing Solarbio Science & Technology Co., Ltd.) containing 20 ml penicillin-streptomycin. The joints were then washed twice with PBS and placed in Dulbecco's modified Eagle's medium (DMEM; Gibco; Thermo Fisher Scientific, Inc.) containing 2 mg/ml type II collagenase for ~8 h at 37°C. The next day, chondrocytes were harvested by filtering through a 70- $\mu$ m cell strainer, washed twice with DMEM, and seeded into a 10-cm cell culture dish (Labserve; Thermo Fisher Scientific, Inc.) with DMEM containing 10% FBS (Gibco; Thermo Fisher Scientific, Inc.), 1% insulin-transferrin-selenium (cat. no. ITSS-10201; Cyagen Biosciences, Inc.) and 1% penicillin-streptomycin, and placed in a 37°C incubator containing 5% CO<sub>2</sub>. The culture medium was replaced every 2 days. All cells were mycoplasma free. Chondrocytes at passages 2-4 were used for the subsequent experiments.

**Evaluation of cell viability.** The effect of AZ on the viability of chondrocytes was evaluated by CCK-8 assay. mouse ATDC5 cells and rat chondrocytes were used for double validation in this experiment, and they were treated using the same conditions. Briefly, chondrocytes were seeded in 96-well plates at a density of 3x10<sup>3</sup>/well. To examine the rescue effect of AZ on chondrocytes in the inflammatory environment, chondrocytes were pretreated with 20 ng/ml rat IL-1 $\beta$  for 24 h, and were then treated with AZ (25, 50 and 100  $\mu$ M) for 24 or 48 h at 37°C. The cells were then incubated with 10% CCK-8 reagent for 2 h at 37°C. In the control group, chondrocytes were treated with 0.1% DMSO (cat. no. D8371; Beijing Solarbio Science & Technology Co., Ltd.), as AZ was dissolved in DMSO. The absorbance at 450 nm was measured immediately using an Epoch microplate reader (BioTek Instruments, Inc.).

**EdU staining.** To directly evaluate chondrocyte proliferation, EdU staining was performed. After the cells were seeded for 8 h on coverslips in a 12-well plate (6x10<sup>3</sup> cells/well), they were pretreated with IL-1 $\beta$  (20 ng/ml) for 24 h and were then treated with different concentrations of AZ (25, 50 and 100  $\mu$ M) for another 24 h at 37°C. For EdU analysis, the 10-mM stock solution was diluted to an appropriate working concentration (1X) with complete medium before starting the experiment. An EdU working solution was added to the 6-well plate, and the cells were incubated for an additional 2 h at 37°C. After EdU labeling of the cells, the culture medium was removed, 1 ml EdU working solution was added, and the cells were fixed at room temperature for 15 min. The fixative solution was removed, and the cells were washed with PBS three times. Subsequently, the washing solution was removed, and the cells were incubated at room temperature for 10-15 min in 1 ml permeabilization solution (PBS containing 0.3% Triton X-100) per well. The cells were washed with PBS, and 0.5 ml Click reaction solution (Beyotime Institute of Biotechnology) was added to each well and incubated at room temperature for 30 min in the dark. After washing with PBS three times, 1 ml 1X Hoechst 33342 solution was added to each well, and the cells were incubated at room temperature for 10 min in the dark. The cells were washed with PBS a further three times (3-5 min/wash) and fluorescence detection was then performed. Hoechst 33342 is a blue fluorescent dye. EdU has a maximum excitation wavelength of 346 nm and a maximum

emission wavelength of 460 nm. Images were captured using a CX41-32RFL inverted fluorescence microscope (Olympus Corporation).

**Crystal violet staining.** To measure the number of chondrocytes, cells were seeded in 6-well plates, pretreated with IL-1 $\beta$  (20 ng/ml) for 24 h, and then treated with different concentrations of AZ (25, 50 and 100  $\mu$ M) for another 24 h at 37°C. The culture medium was discarded, the cells were carefully washed twice with PBS, and 0.5 ml 4% paraformaldehyde solution was added to each well to fix the cells for 30 min at 20°C. The paraformaldehyde solution was aspirated, 0.5 ml 50% crystal violet staining solution was added to each well, and the plate was incubated at room temperature for 20 min. The staining solution was gently removed by shaking, each well was washed with distilled water, and the culture plate was placed upside down on absorbent paper to absorb the water. The plate was then dried at room temperature for 20 min. The 6-well plate was then scanned using an Epson Perfection V370 photograph scanner (Epson).

**Toluidine blue staining.** To measure the ECM content in chondrocytes, cells were seeded in 6-well plates, pretreated with IL-1 $\beta$  (20 ng/ml) for 24 h at 37°C, and then treated with different concentrations of AZ (0, 50 or 100  $\mu$ M) for another 24 h at 37°C. The culture medium was then removed, and cells were carefully washed twice with cold PBS and fixed with 0.5 ml 4% paraformaldehyde solution for 30 min at 20°C. Paraformaldehyde was aspirated and 0.5 ml crystal violet staining solution was added to each well, before the cells were incubated for 20 min at 20°C. After removing the staining solution, each well was washed with distilled water, and the culture plate was placed upside down on absorbent paper to absorb the water and was dried naturally. The 6-well plate was then scanned using an Epson Perfection V370 photograph scanner (Epson).

**Calcein/PI cell viability and cytotoxicity detection.** Rat chondrocytes were seeded in 6-well plates (3x10<sup>4</sup> cells/well), and the cell status was observed after the cells had adhered to the wall, after which the cells were pretreated with IL-1 $\beta$  (20 ng/ml) or Fer-1 (60 nmol/ml) for 24 h, and then treated with or without AZ (100  $\mu$ M) for 24 h at 37°C. After treatment, the culture medium was aspirated, and the cells were washed 1-2 times with PBS. After washing, Calcein AM/PI working solution (1 ml/well) was added, and the cells were incubated at 37°C for 30-60 min in the dark. Subsequently, staining was observed under a fluorescence microscope (Calcein AM emits green fluorescence, whereas PI emits red fluorescence). Images of the cells were captured under a fluorescence microscope (CX41-32RFL; Olympus Corporation).

**Flow cytometry.** Flow cytometry was performed to analyze the apoptotic rate of mouse ATDC5 cells and rat chondrocytes. Cells were seeded in 6-well plates at a density of 1x10<sup>5</sup> cells/well, stimulated with or without IL-1 $\beta$  (20 ng/ml) for 24 h, and then incubated with AZ (100  $\mu$ M) for another 24 h at 37°C. The culture medium was aspirated, the cells were rinsed with 2 ml PBS, and EDTA-free trypsin was added to digest the cells. The cells were gently transferred to

15-ml centrifuge tubes and centrifuged at 1,000 x g for 5 min at 20°C. The supernatant was discarded and the cells were gently resuspended in 195  $\mu$ l binding solution. Subsequently, 5  $\mu$ l Annexin V-FITC and 10  $\mu$ l PI staining solution was added and mixed gently. The samples were incubated at room temperature in the dark for 20 min. Finally, the samples were immediately analyzed with a BD FACSCalibur flow cytometer (BD Biosciences). Data were analyzed using FlowJo 10 for Mac v10.4 (FlowJo, LLC).

**Measurement of ROS levels.** Cells were first treated as described for crystal violet staining, and a commercially available ROS detection kit was used to measure intracellular ROS levels in the chondrocytes. The DCFH-DA probe was diluted in serum-free medium (1:1,000) to a final concentration of 10  $\mu$ M. The culture medium was removed, and 1 ml diluted DCFH-DA was added to each well and the cells were incubated for 20 min at 37°C. The cells were rinsed three times with serum-free culture medium to fully remove the excess DCFH-DA, and were then immediately observed and photographed under a CX41-32RFL fluorescence microscope (Olympus Corporation).

**Malondialdehyde (MDA) assay.** MDA concentration was evaluated using an MDA assay kit (cat. no. MAK085; MilliporeSigma) according to the manufacturer's instructions. Rat and mouse cells were used for double validation in this experiment, and they were treated using the same conditions. Cells were seeded in 6-well plates at a density of  $1 \times 10^5$  cells/well, stimulated with or without IL-1 $\beta$  (20 ng/ml) for 24 h, and then incubated with AZ (100  $\mu$ M) or Fer-1 (60 nmol/ml) for another 24 h at 37°C. Cells ( $1 \times 10^6$ ) were homogenized on ice in 300  $\mu$ l MDA lysis buffer containing 3  $\mu$ l 2-methyl-2-propenoic acid (100X). The samples were centrifuged at 13,000 x g for 10 min at 20°C to remove any insoluble material, after which 600  $\mu$ l thiobarbituric acid solution was added to each sample. The samples were incubated at 95°C for 60 min and cooled to room temperature in an ice bath for 10 min. Finally, 200  $\mu$ l reaction mixture was pipetted into a 96-well plate and the absorbance was measured at 532 nm.

**Glutathione (GSH) assay.** GSH concentration was measured using a total GSH assay kit (cat. no. BC1175; Beijing Solarbio Science & Technology Co., Ltd.) according to the manufacturer's protocol. Rat and mouse cells were used for double validation in this experiment, and they were treated using the same conditions. Cells were seeded in 6-well plates at a density of  $1 \times 10^5$  cells/well, stimulated with or without IL-1 $\beta$  (20 ng/ml) for 24 h, and then incubated with AZ (100  $\mu$ M) or Fer-1 (60 nmol/ml) for another 24 h at 37°C. A total of  $1 \times 10^7$  cells were washed with PBS and then centrifuged at 600 x g for 5 min at 20°C to obtain a compact cell pellet. The supernatant was removed, and three volumes of a 5% sodium thiosulfate solution were added to the cell pellet and vortexed. The suspension was freeze-thawed twice (liquid nitrogen was used for freezing and a 37°C water bath was used for thawing) and left for 5 min at 2-8°C. The extract was then centrifuged at 10,000 x g for 10 min at 20°C and 200  $\mu$ l was added to a 96-well plate to measure the absorbance at 412 nm.

**Western blot analysis.** Cells were processed using a method similar to that used for EdU staining. Subsequently, the cells were washed three times with cold PBS and lysed for 20 min on ice with RIPA buffer (Beyotime Institute of Biotechnology) containing a 10% phosphatase and protease inhibitor cocktail (complete, EDTA-free; Roche Applied Science) and PMSF (Beyotime Institute of Biotechnology). The lysate and loading buffer (Beyotime Institute of Biotechnology) were mixed in a 1X ratio, heated in a 100°C water bath for 5 min, and then maintained at -80°C until further use. The proteins (20  $\mu$ g) were separated by SDS-PAGE on 8-12% gels and transferred to polyvinylidene fluoride (PVDF) membranes, which were blocked in 5% skim milk at room temperature for 1 h. The PVDF membranes were then incubated with primary antibodies for 10 h at 4°C and were then incubated with 1:8,000 secondary antibodies at room temperature for 1 h. ECL chemiluminescent imaging was performed, and the proteins were immediately visualized with an Amersham 600 chemiluminescence system (Cytiva) and analyzed by ImageJ V 1.8.0 (National Institutes of Health). The following primary and secondary antibodies were used in the present study: Nrf2 (cat. no. 16396-1-AP; 1:2,000), HO-1 (cat. no. 10701-1-AP; 1:1,000), GPX4 (cat. no. 67763-1-Ig; 1:2,000), ADAMTS-4 (cat. no. 11865-1-AP; 1:500), inducible nitric oxide synthase (iNOS; cat. no. 18985-1-AP; 1:1,000), MMP13 (cat. no. 18165-1-AP; 1:1,000), cyclooxygenase 2 (COX2; cat. no. 27308-1-AP; 1:1,000), aggrecan (cat. no. 13880-1-AP; 1:1,000), collagen type II  $\alpha$ 1 (COL2A1; cat. no. 28459-1-AP; 1:1,000), Notch1 (cat. no. 20687-1-AP; 1:1,000), suppressor of cytokine signaling 3 (SOCS3; cat. no. 14025-1-AP; 1:1,000) and  $\beta$ -actin (cat. no. 66009-1-Ig; 1:4,000) (all from Proteintech Group Inc.), and caspase 3 (cat. no. A0214; 1:1,000) and cleaved caspase 3 (cat. no. A19654; 1:1,000) (both from ABclonal Biotech Co., Ltd.) primary antibodies; HRP-conjugated AffiniPure goat anti-rabbit IgG (H+L) (cat. no. SA00001-2; 1:8,000) and HRP-conjugated AffiniPure goat anti-mouse IgG (H+L) (cat. no. SA00001-1; 1:8,000) secondary antibodies (both from Proteintech Group Inc.).

**Transmission electron microscopy (TEM).** Cells were seeded in 6-well plates at a density of  $1 \times 10^5$  cells/well, stimulated with or without IL-1 $\beta$  (20 ng/ml) for 24 h, and then incubated with AZ (100  $\mu$ M) or Fer-1 (60 nmol/ml) for another 24 h at 37°C. Chondrocytes were fixed in 2.5% glutaraldehyde in 0.05 M sodium cacodylate buffer (pH 7.2) for 2 h at 25°C, followed by 2 h in 2% OsO<sub>4</sub> in 0.1 M cacodylic acid sodium buffer, and incubation with 1% uranyl acetate aqueous solution for 18 h at 25°C. After dehydration through an ethanol series, the specimens were embedded in Epon 812, and 5  $\mu$ m sections were collected on copper plates. After staining with 50% uranyl acetate and 30-40 g/l lead citrate for 2 h at 25°C, the sections were examined using an electron microscope (HT7800; Hitachi, Ltd.).

**Induction of a knee OA model by destabilization of the medial meniscus (DMM) surgery in mice.** A total of 20 2-month-old male C57BL/6J mice (weight, 20 g) were purchased from Changzhou Laboratory Animal Company and were fed commercial food and water under specific pathogen-free conditions. The mice were maintained at 20-25°C and 50-60% humidity, had free access to pure water and special feed, and

were kept under a 12-h light/dark cycle. The present study was approved by the Animal Ethical Committee of Nanjing Medical University (Changzhou, China); all animal experiments complied with the National Institutes of Health Guide for the Care and Use of Laboratory Animals (45). Mice were sacrificed by CO<sub>2</sub> asphyxiation (fill rate, 60% chamber volume/min), and death was confirmed by observing a lack of respiration and faded eye color (46,47). The method of sacrifice used is able to fulfill the objective of rapid unconsciousness with minimal distress to the animals (47). The mice were anesthetized by intraperitoneal injection of pentobarbital sodium (50 mg/kg) before surgery. DMM surgery was performed on the right knee of the mice to surgically induce an OA model. DMM-induced abnormal mechanical loading-associated OA of the right knee was established according to a previous study (35). The 20 mice were randomly divided into four groups (n=5/group) and all of the mice were maintained for 4 weeks after surgery. The groups were as follows: i) The control group, in which the joint capsule was opened, and the incision was sutured; ii) the DMM group, in which the mice were injected with PBS in the joints once every other day for 4 weeks after DMM surgery; iii) 0.25 and iv) 1 mg/kg body weight AZ groups, in which the mice were injected with AZ by intra-articular injection once every other day for 4 weeks.

**Micro-CT scanning and analysis.** After the mice were sacrificed, the whole hind limbs were collected and fixed in 10% neutral buffered formalin for 24 h at 20°C, and the excess soft tissue was removed. The whole hind limbs were scanned using a Skyscan 1276 micro-CT instrument (Bruker Belgium SA) using the following settings: Source voltage, 55 kV; source current, 200  $\mu$ A; 0.25-mm filter; pixel size, 6  $\mu$ m; and rotation step, 0.3 degrees. The images were then reconstructed with NRecon V 1742 software (Bruker Belgium SA); the target area was the knee joint. The three-dimensional structural parameters that were analyzed were bone volume (BV), total volume (TV), their ratio (BV/TV), trabecular number (Tb. N), and trabecular thickness (Tb. Th).

**Immunohistochemical staining.** After all mice were sacrificed, the whole hind limbs were decalcified in 10% EDTA/PBS and then embedded in paraffin. All samples were fixed in 4% paraformaldehyde for 24–48 h. Sagittal sections of the knee joint medial compartment were cut to a 4- $\mu$ m thickness and were stained with hematoxylin & eosin (H&E) and Safranin O/Fast Green (S&F) for 24 h at 20°C. Staining was evaluated using the Osteoarthritis Research Society International (OARSI) method and OARSI 2019 guidelines (48). Immunohistochemical staining was performed with antibodies against Nrf2, GPX4, and aggrecan (1:200; Proteintech Group, Inc.) for 2 h at 4°C. Tissues (4  $\mu$ m) were fixed in 4% paraformaldehyde for 24 h at 20°C, then dehydrated in a descending ethanol series and permeabilized in xylene before being embedded in paraffin at 20°C. Samples were also stained with diaminobenzidine (Dako; Agilent Technologies, Inc.) and counterstained with hematoxylin (MilliporeSigma) for 24 h at 20°C. Images were captured using a Zeiss Axio Imager light microscope (Zeiss AG).

**Statistical analysis.** All quantitative data are presented as the mean  $\pm$  standard deviation or as median and IQR. The *in vitro*

experiments were repeated three times. Statistical analysis was performed using GraphPad Prism 7 software (Dotmatics). One-way ANOVA and Tukey's multiple comparisons test was used to analyze the significance of differences among the groups. Kruskal-Wallis test and Dunn's post hoc test was used to analyze the significant differences in OARSI score.  $P < 0.05$  was considered to indicate a statistically significant difference.

## Results

**AZ relieves osteophyte formation in mice following DMM surgery.** The chemical structure of AZ is shown in Fig. 1A. To exclude false positives caused by impurities, the NMR spectrum of AZ was obtained to verify the purity of the compound that was used. The NMR results showed that the purity of AZ was >98% (Fig. 1B). To investigate the effects of AZ on cartilage destruction and osteophyte formation in OA, mice were intra-articularly injected with AZ after DMM surgery. The results showed that DMM surgery caused bone destruction; however, AZ treatment dose-dependently reduced cartilage destruction, increasing the integrity of the kneecap and cartilage mass in the subchondral cartilage (Fig. 1C and D). The BV of the tibial plateau subchondral cartilage in the DMM group was  $2.14 \pm 0.06$  mm<sup>3</sup>, which was significantly lower than that in the control group ( $2.60 \pm 0.08$  mm<sup>3</sup>). In mice treated with 0.25 and 1 mg/kg AZ, the BV was  $2.27 \pm 0.07$  and  $2.39 \pm 0.05$  mm<sup>3</sup>, respectively, but there were no significant differences between the two groups (Fig. 1E). It can be seen from the results that after DMM surgery, bone destruction increased, BV decreased, and the BV/TV (Fig. 1F), Tb. N (Fig. 1G) and Tb. Th (Fig. 1H) were decreased. In the AZ treatment groups, osteophytes decreased, bone volume increased, and Tb. N and Tb. Th increased accordingly. There was no significant difference in bone volume and trabecular thickness in the AZ low-dose group compared with in the DMM group. The BV and other parameters, including BV/TV, Tb. N and Tb. Th, indicated that AZ inhibited the increase in osteophytes induced by DMM surgery.

**AZ promotes chondrocyte proliferation and maintains ECM homeostasis *in vitro*.** The results of a CCK-8 assay showed that AZ at concentrations of 25, 50 and 100  $\mu$ M had no cytotoxic effects and promoted the viability of chondrocytes after 24 and 48 h compared with the IL-1 $\beta$ -treated group (Fig. 2A). In addition, similar results were obtained in the mouse cell line ATDC5 (Fig. S1A). Furthermore, EdU staining showed that the decrease in the proliferation of chondrocytes following IL-1 $\beta$  treatment was reversed by AZ in a dose-dependent manner (Fig. 2B). Subsequently, the effect of AZ on the expression levels of cartilage ECM proteins were determined. After IL-1 $\beta$  treatment, aggrecan and COL2A1 were significantly reduced compared with in the control group, whereas AZ significantly promoted aggrecan and COL2A1 expression compared with that in the IL-1 $\beta$  group, which was beneficial for maintaining the integrity of the articular cartilage (Fig. 2C and E). In addition, western blotting showed that AZ inhibited the expression levels of inflammatory factors (iNOS and COX2) and inhibited the expression of matrix-degrading enzymes (ADAMTS-4 and MMP13) in IL-1 $\beta$ -treated chondrocytes (Fig. 2D and E). These data suggested that AZ may inhibit inflammatory factor-induced degradation of ECM proteins to maintain cartilage integrity.



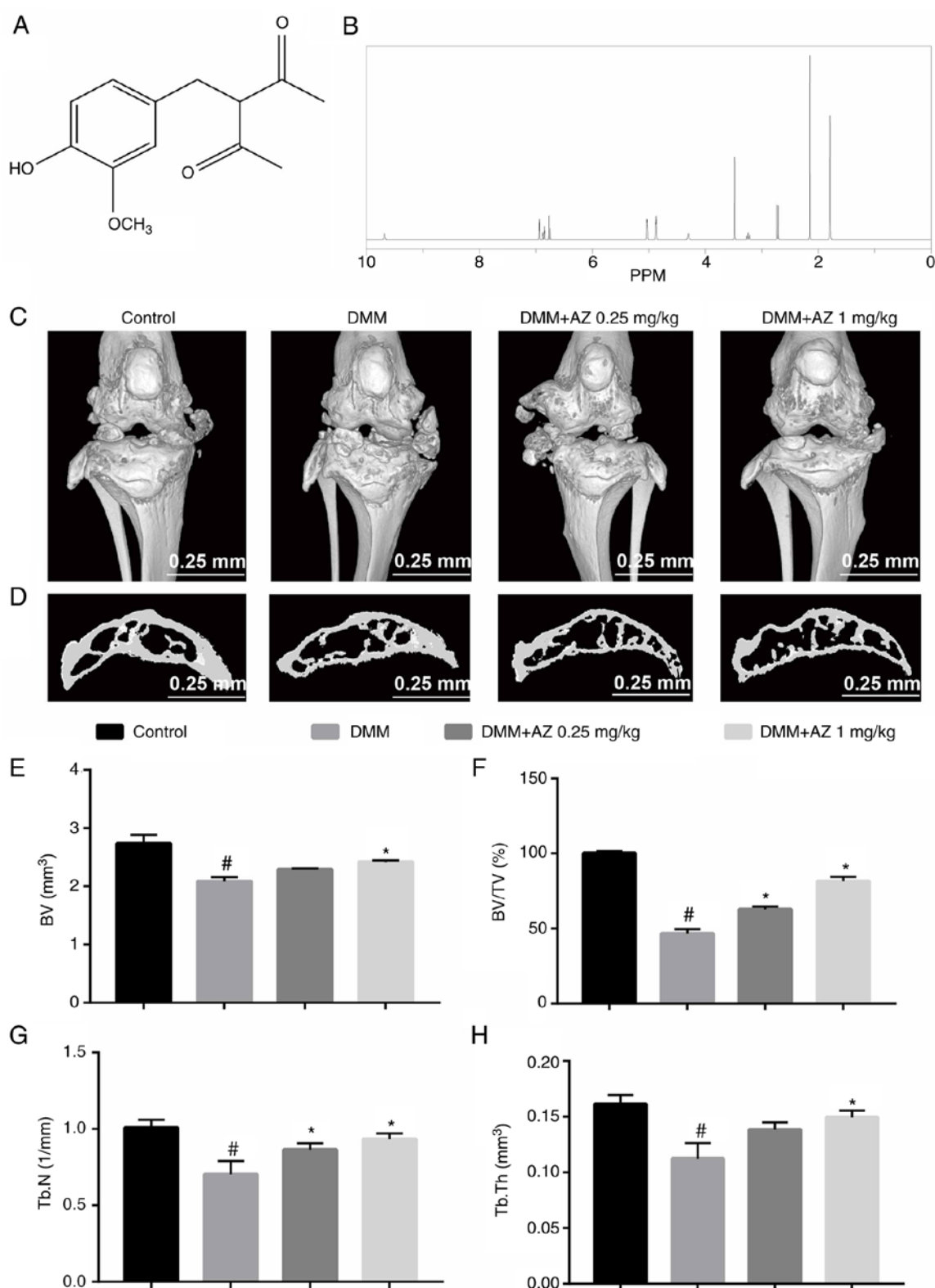


Figure 1. Micro-CT evaluations of AZ-treated OA induced by DMM surgery. (A) Chemical structure of AZ. (B) Nuclear magnetic resonance spectrum of AZ. (C) Micro-CT images of frontal views of the knee joints at 4 weeks after sham or DMM operation. (D) Sagittal views of the medial compartment subchondral bone. Quantitative analysis of (E) BV, (F) BV/TV, (G) Tb. N and (H) Tb. Th. # $P < 0.05$  vs. control; \* $P < 0.05$  vs. DMM. AZ, acetyl zingerone; BV, bone volume; DMM, destabilization of the medial meniscus; Tb. N; trabecular number; Tb. Th, trabecular thickness; TV, total volume.

*AZ maintains ECM homeostasis in vivo.* Following treatment with AZ, both H&E (Fig. 3A) and S&F staining (Fig. 3B) showed that AZ could promote cartilage repair and reduce bone loss in the DMM group. H&E and S&F staining demonstrated the

loss of proteoglycans and decreased thickness of the articular cartilage caused by DMM surgery (Fig. 3A and B). From the results, it can be concluded that the content of aggrecan in the DMM group was significantly lower than that in the control

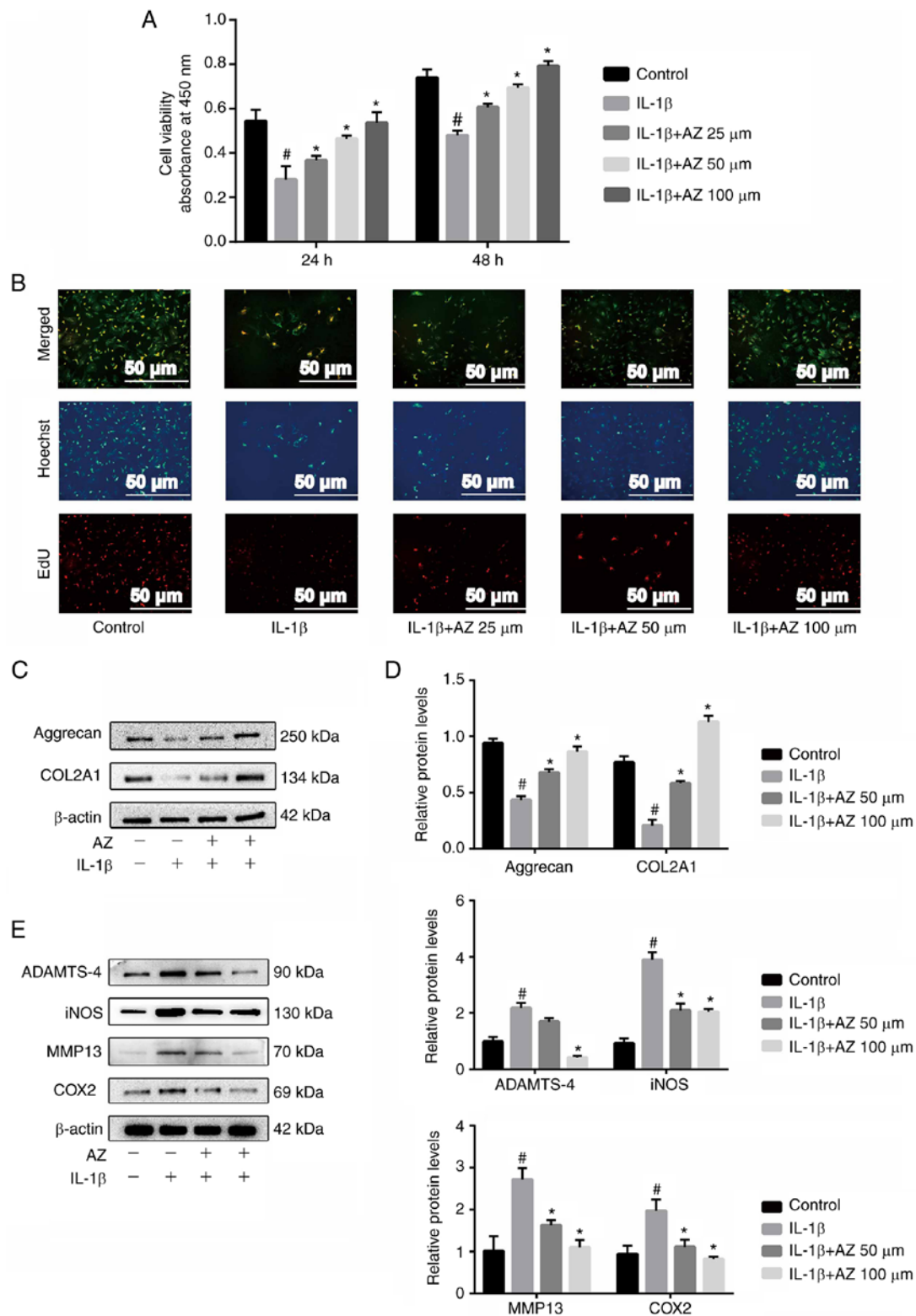


Figure 2. AZ promotes chondrocyte proliferation, and inhibits the expression of inflammatory factors and matrix-degrading enzymes. Chondrocytes were pretreated with DMSO and IL-1 $\beta$  (20 ng/ml) for 24 h, and were then treated with AZ (25, 50 and 100  $\mu$ M) for another 24 or 48 h. (A) Cell viability was assessed using the Cell Counting Kit-8 assay. (B) EdU staining (red fluorescence) was used to assess cell proliferation. (C) Expression levels of aggrecan and COL2A1. (D) ImageJ was used to analyze the relative protein expression levels of aggrecan, COL2A1, ADAMTS-4, iNOS, MMP13 and COX2. (E) ADAMTS-4, iNOS, MMP13 and COX2 were detected by western blotting. \* $P$ <0.05 vs. control; # $P$ <0.05 vs. IL-1 $\beta$ . AZ, acetyl zingerone; COL2A1, collagen type II  $\alpha$ 1; COX2, cyclooxygenase 2; EdU, 5-ethynyl-2'-deoxyuridine; iNOS, inducible nitric oxide synthase.

group. Compared with in the DMM group, there was a significant increase in aggrecan in the AZ group (Fig. 3C and D). Moreover, OARSI was significantly increased in the DMM

group compared with that in the control group. Compared with in the DMM group, there was a significant decrease in OARSI in the AZ group (Fig. 3E).

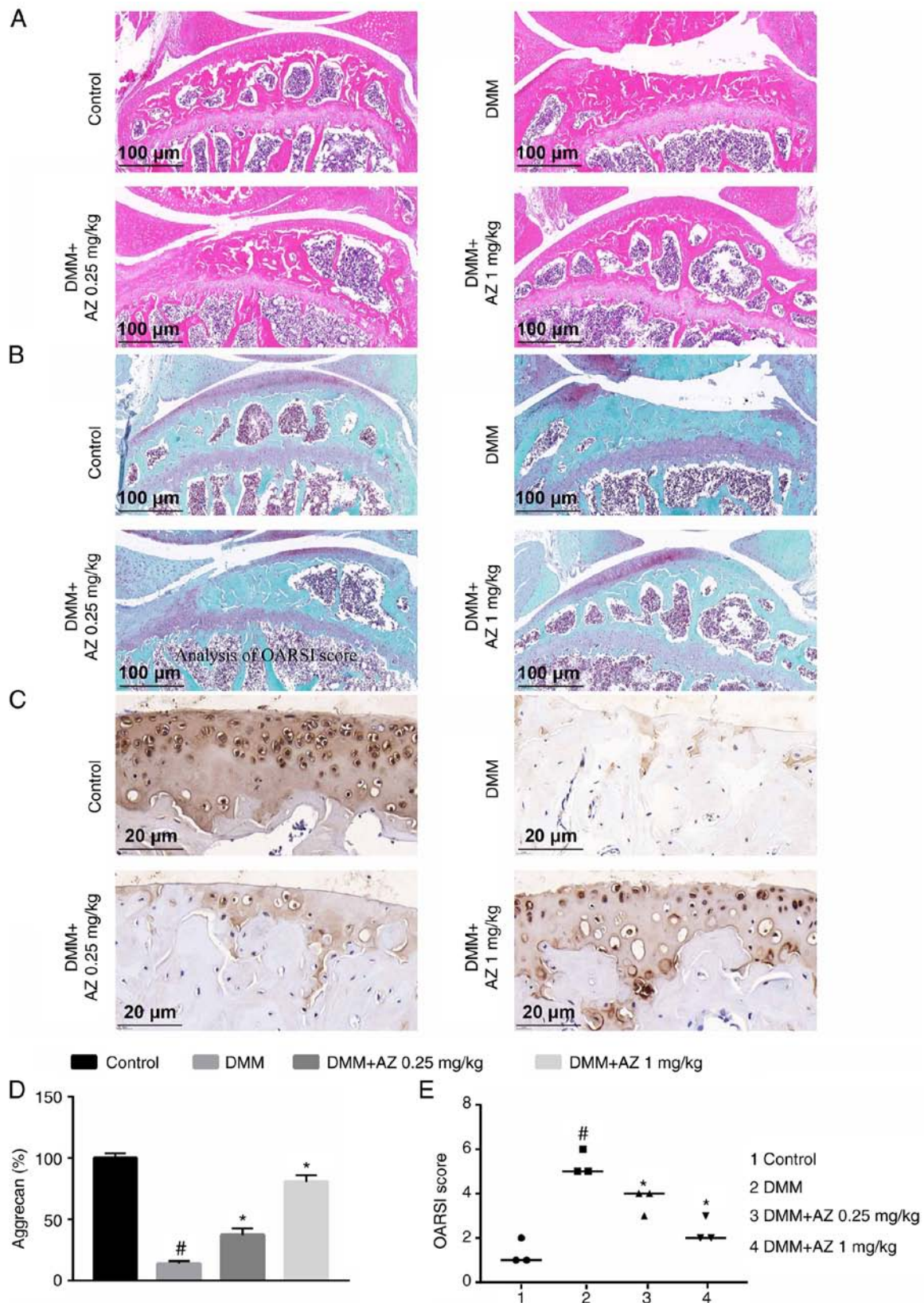


Figure 3. AZ inhibits cartilage degeneration in DMM mice. Medial compartment cartilage and subchondral bone of the knee stained with (A) hematoxylin and eosin and (B) Safranin O/Fast Green. (C) Aggrecan immunohistochemistry of cartilage in the knee joint medial compartment. (D) Area calculation of aggrecan expression. (E) Analysis of OARSI score. \* $P < 0.05$  vs. control; # $P < 0.05$  vs. DMM. AZ, acetyl zingerone; DMM, destabilization of the medial meniscus; OARSI, Osteoarthritis Research Society International.

*AZ inhibits chondrocyte apoptosis and promotes Notch1 expression.* Chondrocyte apoptosis caused by chronic

inflammation in OA is an important factor in the progression of the disease (42). The results of crystal violet staining showed



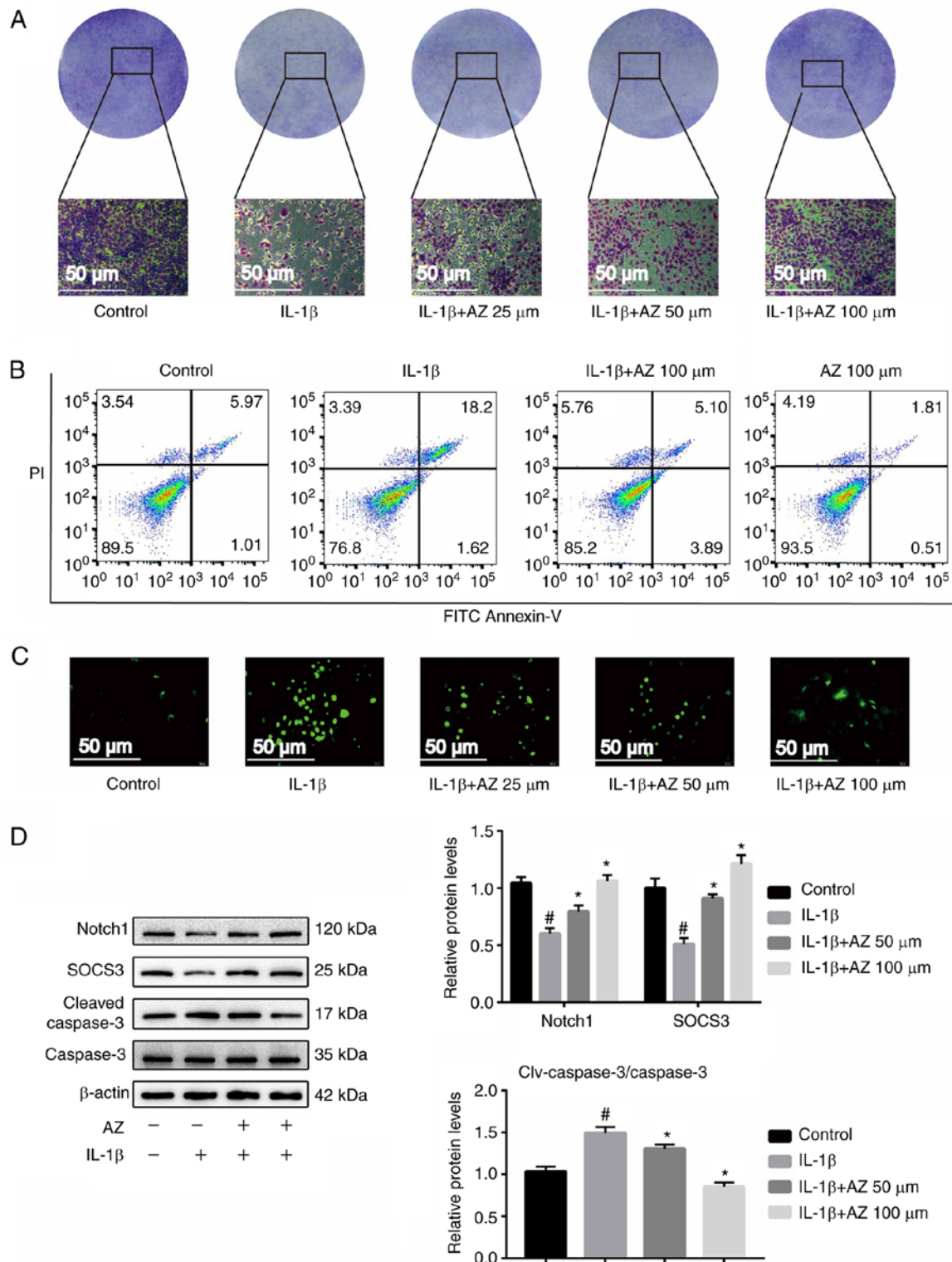


Figure 4. AZ inhibits IL-1 $\beta$ -induced chondrocyte apoptosis by promoting Notch1 expression. Chondrocytes were pretreated with or without IL-1 $\beta$  (20 ng/ml) for 24 h and were then treated with AZ (25, 50 or 100  $\mu$ M) for an additional 24 h. (A) Cells were visualized with crystal violet staining. (B) Chondrocyte apoptosis was measured by flow cytometry. (C) ROS levels. (D) Chondrocytes were pretreated with or without IL-1 $\beta$  (20 ng/ml) for 24 h and were then treated with AZ (50 or 100  $\mu$ M) for an additional 24 h. Expression of Notch1, SOCS3, caspase 3 and Cleaved caspase 3 was determined by western blotting, and ImageJ was used to analyze relative protein expression levels. <sup>#</sup>P<0.05 vs. control; <sup>\*</sup>P<0.05 vs. IL-1 $\beta$ . AZ, acetyl zingerone; SOCS3, suppressor of cytokine signaling 3.

that the number of chondrocytes in the IL-1 $\beta$  group was reduced compared with the control group, whereas AZ treatment inhibited this trend, and the number of chondrocytes was increased compared with the IL-1 $\beta$  group (Fig. 4A). Similar results were obtained from the mouse cell experiments. From

the results of toluidine blue staining, after treatment with IL-1 $\beta$ , the content of the ECM was markedly reduced, whereas it was increased after AZ compared with that in the IL-1 $\beta$  group (Fig. S1C). As determined by flow cytometry, the proportion of early + late apoptotic cells in the IL-1 $\beta$ -induced group was

markedly increased compared with that in the control group. By contrast, compared with in the IL-1 $\beta$  group, the AZ treatment groups exhibited reduced apoptosis, thus indicating that AZ may have a marked effect on inhibiting the apoptosis of chondrocytes. (Fig. 4B). In addition, similar results were obtained in the mouse cell line ATDC5 (Fig. S1B). These findings indicated that AZ could reverse the increase in apoptosis induced by IL-1 $\beta$ . The results of ROS analysis revealed that in the IL-1 $\beta$  group, a marked accumulation of ROS was detected compared with that in the control group; however, compared with in the IL-1 $\beta$  group, AZ markedly reduced the accumulation of ROS (Fig. 4C).

It has previously been reported that Notch signaling activation contributes to the synthesis of the chondrocyte matrix and promotes joint repair (49,50). In addition, the inhibition of Notch signaling can significantly reduce the proliferation of OA chondrocytes (51). Therefore, normal Notch expression is important for chondrocytes. Notably, SOCS3 has been identified as a pivotal regulator of the Notch pathway, which is involved in multiple physiological processes (52). SOCS3 is a downstream protein of the Notch pathway, which can reflect the activation of Notch. Notch1 is the active state of Notch, which indicates activation of the Notch pathway. The present results showed that the expression levels of the key factor Notch1 (cleaved Notch) and SOCS3 in the Notch pathway were significantly decreased (Figs. 4D and S1D), and the cleaved caspase-3/caspase-3 ratio was increased following treatment with IL-1 $\beta$ , whereas AZ significantly increased Notch1 and SOCS3 expression, and decreased the cleaved caspase-3/caspase-3 ratio (Fig. 4D). In addition, similar results were determined in the mouse cell line ATDC5 (Fig. S1D). Therefore, AZ may inhibit chondrocyte apoptosis through the Notch pathway.

*AZ inhibits chondrocyte ferroptosis.* MDA and GSH are considered key effective metabolic indicators involved in the regulation of ferroptosis (53). IL-1 $\beta$  is used as a classic inducer of OA *in vitro*, and recent studies have demonstrated that it also induces ferroptosis in chondrocytes (24-26). Fer-1 is a specific inhibitor of ferroptosis, which was used as a control to confirm the effect of AZ. The present results showed that IL-1 $\beta$  induced a decrease in GSH levels and an increase in MDA levels; however, these effects were alleviated by the addition of AZ and Fer-1 (60 nmol/ml) (Fig. 5A and B); AZ significantly increased the levels of GSH in chondrocytes and reduced the accumulation of MDA. In addition, similar results were obtained in the mouse cell line ATDC5 (Fig. S2A and B). A reduction in or the disappearance of mitochondrial cristae is a characteristic indicator of ferroptosis (54). TEM was used to examine the morphological changes characteristic of ferroptosis. In the IL-1 $\beta$  group, the mitochondrial morphology was markedly altered, the size of the mitochondria decreased, the density of the double membrane increased, the outer membrane of the mitochondria was broken and the mitochondrial ridge disappeared, which were all signs of ferroptosis. By contrast, AZ or Fer-1 (60 nmol/ml) markedly inhibited these morphological changes, and stabilized the structure and shape of mitochondria (Fig. 5C). Calcein/PI cell viability and cytotoxicity assay results showed that after IL-1 $\beta$  induction, the proportion of dead cells was increased and the live number

of rat chondrocytes was decreased. Treatment with AZ or Fer-1 (60 nmol/ml) inhibited the ferroptosis of chondrocytes (Fig. 5D). Subsequently, western blotting showed that the expression levels of GPX4, a key protein involved in ferroptosis, were significantly decreased in the IL-1 $\beta$  group, whereas AZ and Fer-1 (60 nmol/ml) promoted the expression of GPX4, which in turn may protect chondrocytes from ferroptosis (Fig. 5E); similar results were determined in the mouse cell line ATDC5 (Fig. S2C). Furthermore, immunohistochemical staining confirmed that the expression of GPX4 was reduced in the DMM mice, whereas AZ promoted its expression (Fig. 5F). Taken together, these findings suggested that AZ may inhibit ferroptosis.

#### *AZ inhibits ferroptosis in OA through the Nrf2/HO-1 pathway.*

The results of western blotting showed that both Nrf2 and HO-1 were markedly increased in the IL-1 $\beta$  group, indicating that ferroptosis occurred in chondrocytes, and Nrf2 and HO-1 responded to this change. By contrast, AZ and Fer-1 (60 nmol/ml) markedly promoted the expression levels of Nrf2 and HO-1 compared with those in the IL-1 $\beta$  group (Fig. 6A and B). To explore this finding further, inhibitors of Nrf2 (ML385) and HO-1 (tin protoporphyrin IX) were used. IL-1 $\beta$ -suppressed the expression levels of GPX4. The application of these inhibitors exacerbated the IL-1 $\beta$ -induced suppression of GPX4. Moreover, the anti-ferroptosis effect of AZ was also abolished. GPX4 is a downstream protein of Nrf2 and HO-1. When Nrf2 and HO-1 are inhibited, intracellular antioxidant substances will decrease, and the expression of GPX4 will increase accordingly (55). However, due to the increased levels of oxidative stress substances, such as ROS, GPX4 will reduce. From the results, it can be seen that the expression of GPX4 was decreased following treatment with the Nrf2 inhibitor. Since HO-1 is regulated by Nrf2, the expression of HO-1 was also reduced after Nrf2 inhibitor treatment (Fig. 6A). In addition, the expression of GPX4 was decreased following treatment with the HO-1 inhibitor. The result of Nrf2 immunohistochemical staining showed that the levels of Nrf2, which is in the ferroptosis pathway (56), were increased in the DMM group, whereas AZ treatment further promoted Nrf2 expression (Fig. 6B). Since Nrf2 is not regulated by HO-1, the expression of Nrf2 was not affected by HO-1 inhibitor treatment (Fig. 6C). The potential mechanism by which AZ inhibits chondrocyte ferroptosis is shown in Fig. 6D. Taken together, these data suggested that AZ may inhibit ferroptosis in OA through the Nrf2/HO-1 pathway.

## Discussion

OA is a dynamic process caused by the repair and damage of joint tissues (2). The pathogenesis of this disease is complicated, and it involves factors such as inflammation, aging and metabolism, which eventually lead to the destruction of the joint structure (57). An abnormal chondrocyte programmed cell death rate is a major trigger of OA. Results from the present study revealed that AZ inhibited the expression of proinflammatory factors in chondrocytes, thereby reducing the accumulation of ROS. Notch signaling is also closely related to the pathogenesis of OA (58). Long-term inhibition of Notch signal transduction leads to an imbalance in cartilage

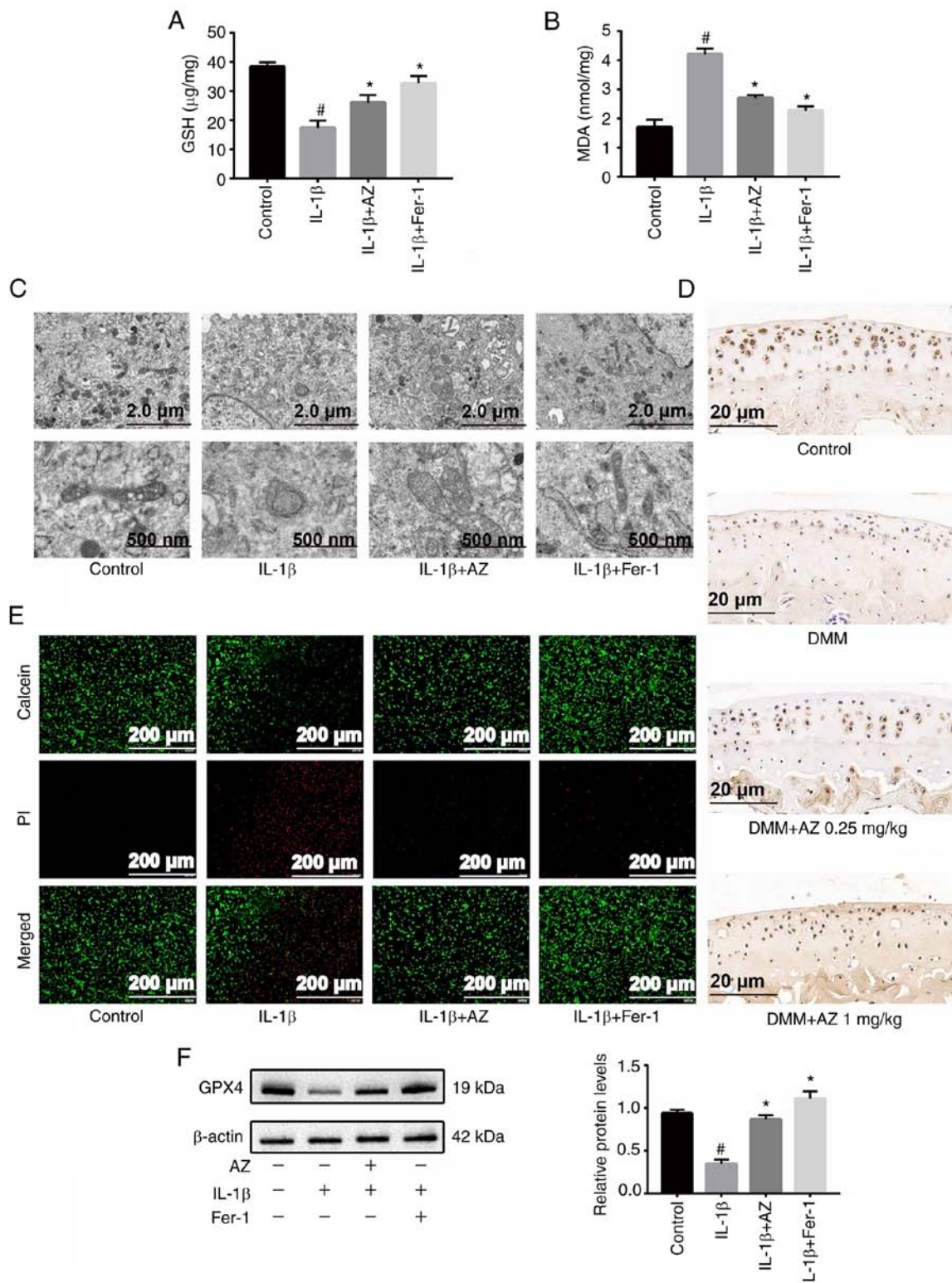


Figure 5. AZ inhibits IL-1 $\beta$ -induced ferroptosis in chondrocytes. (A) GSH and (B) MDA levels were measured in each group using GSH and MDA assays. Chondrocytes were pretreated with IL-1 $\beta$  (20 ng/ml) or Fer-1 (60 nmol/ml) for 24 h and then treated with or without AZ (100  $\mu$ M) for an additional 24 h. (C) Mitochondria were observed by transmission electron microscopy. (D) GPX4 staining to indicate ferroptosis in mice following DMM surgery. (E) Cells were observed by fluorescence microscopy. (F) Chondrocytes were pretreated with or without IL-1 $\beta$  (20 ng/ml) or Fer-1 (60 nmol/ml) for 24 h and then treated with AZ (100  $\mu$ M) for another 24 h, and GPX4 expression was determined by western blotting. <sup>#</sup>P<0.05 vs. control; <sup>\*</sup>P<0.05 vs. IL-1 $\beta$ . AZ, acetyl zingerone; DMM, destabilization of the medial meniscus; Fer-1, ferrostatin-1; GPX4, glutathione peroxidase 4; GSH, glutathione; MDA, malondialdehyde.

homeostasis and the growth of osteophytes (59). The present study found that AZ may promote chondrocyte proliferation by activating the Notch pathway.

Ferroptosis is iron-dependent regulated cell death that is caused by an accumulation of lipid peroxidation products and is prevented by GPX4, a key antioxidant enzyme (60). In



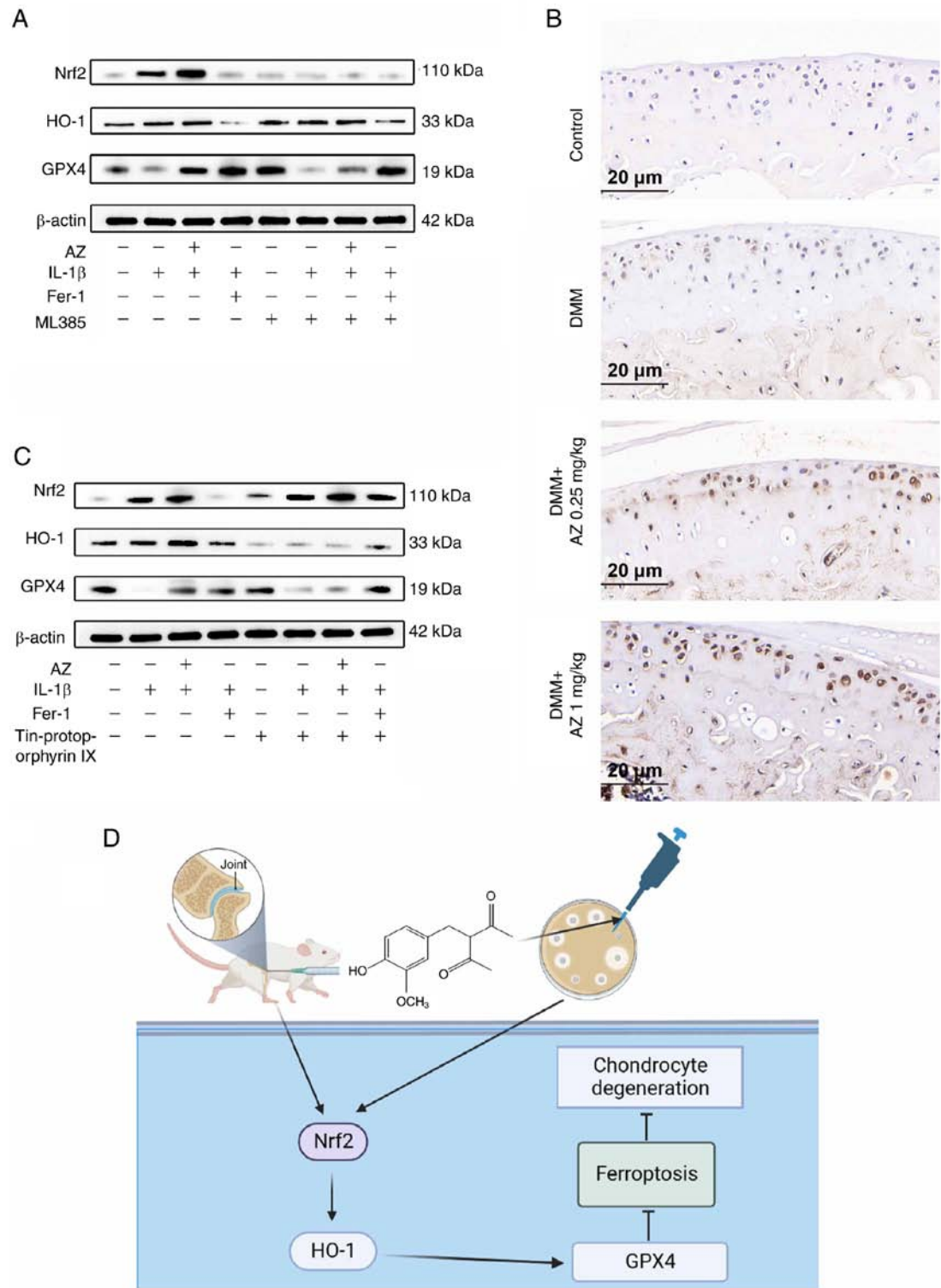


Figure 6. AZ inhibits ferroptosis in osteoarthritis through the Nrf2/HO-1 pathway. Chondrocytes were pretreated with IL-1β (20 ng/ml) for 24 h, with or without ML385 (Nrf2 inhibitors) or Fer-1 (60 nmol/ml) for 12 h, and then treated with or without AZ (100 μM) for an additional 24 h. (A) Protein expression levels of Nrf2, HO-1 and GPX4 was determined by western blotting. (B) Nrf2 staining of ferroptosis in chondrocytes. Chondrocytes were pretreated with IL-1β (20 ng/ml) for 24 h, with or without tin protoporphyrin IX (HO-1 inhibitors) or Fer-1 (60 nmol/ml) for 12 h, and then treated with or without AZ (100 μM) for an additional 24 h. (C) Protein expression levels of Nrf2, HO-1 and GPX4 was determined by western blotting. (D) Schematic diagram showing how AZ affects ferroptosis through the Nrf2/HO-1 signaling pathway. AZ, acetyl zingerone; DMM, destabilization of the medial meniscus; Fer-1, ferrostatin-1; GPX, glutathione peroxidase 4; HO-1, heme oxygenase-1; Nrf2, nuclear factor erythroid 2-related factor 2.

previous years, chondrocyte ferroptosis has attracted attention, and effective inhibition of this type of cell death may be a new target in the treatment of OA (61). It has been reported that mechanical overload induces GPX4-regulated chondrocyte

ferroptosis in OA through Piezo1 channel-facilitated calcium influx (62). In the present study, AZ was shown to upregulate the expression of GPX4, thus potentially inhibiting ferroptosis. The present study simulated the microenvironment of OA by



treating chondrocytes with IL-1 $\beta$ . In this model, the expression of GPX4 was significantly decreased, and the chondrocyte mitochondria were markedly deformed or even disappeared. These morphological and protein expression change are consistent with the occurrence of ferroptosis (63). Further study revealed that the features of IL-1 $\beta$ -induced ferroptosis could be reversed by AZ. Furthermore, in the DMM rat model, AZ successfully alleviated joint degeneration and osteophyte formation, and promoted the expression of GPX4. Taken together, the present results suggested that AZ may attenuate the degeneration of cartilage in OA through the inhibition of chondrocyte ferroptosis.

Both Nrf2 and HO-1 are important elements in the antioxidant response to stress (64). When cells are under oxidative stress, corresponding increases in Nrf2 and HO-1 levels induce the expression of downstream genes, thereby enhancing the resistance of cells to oxidative stress or programmed cell death, and maintaining cell stability (65). Previous reports have demonstrated that the Nrf2/HO-1 pathway protects cells from ferroptosis. Notably, increased expression of Nrf2/HO-1 can protect against ferroptosis (66,67). Furthermore, Nrf2/HO-1 serves an important role in regulating the expression of GPX4 in various inflammatory diseases (68), and GPX4 is a downstream molecule of Nrf2 (69). The present study aimed to examine whether Nrf2/HO-1 is essential for the mechanism by which AZ suppressed IL-1 $\beta$ -induced ferroptosis in chondrocytes; therefore, Nrf2 and HO-1 expression levels were assessed *in vitro*. AZ treatment significantly suppressed IL-1 $\beta$  cytotoxicity in osteoarthritic chondrocytes and inhibited IL-1 $\beta$ -induced ferroptosis by promoting Nrf2/HO-1 expression. Moreover, the levels of GPX4, a key inhibitory factor of ferroptosis, were evaluated after the application of Nrf2 or HO-1 inhibitors. The results were consistent with our hypothesis that these inhibitors aggravated the decrease in GPX4 induced by IL-1 $\beta$  and abolished the rescue effect of AZ. These data demonstrated that AZ may inhibit chondrocyte ferroptosis through Nrf2/HO-1. Ferroptosis has broad clinical application prospects in the treatment of OA. The present study demonstrated that AZ treatment may be effective in preventing the death of osteoarthritic chondrocytes. Future preclinical studies are required to assess whether AZ can inhibit the progression of OA.

Considering the consistency of *in vivo* and *in vitro* experiments, mouse ATDC5 cells should preferably have been chosen for *in vitro* experiments; however, rat cells extracted from 8-week-old rats were considered more appropriate for the following reasons (61). First, fully mature and differentiated chondrocytes were required to mimic the *in vivo* OA environment. Second, the number of rat chondrocytes isolated according to the literature is abundant, and the cell viability is excellent (70). According to our observation, signs of aging only appear after >8 passages *in vitro*. Third, it is much easier to separate the articular cartilage with a scalpel from the tibia of an 8-week-old rat than in a mouse, without contaminating other tissues. Finally, 8-week-old rat chondrocytes were used for *in vitro* experiments. Regarding cell selection for *in vitro* models, three types of cells were considered when designing experiments: ATDC5 cells, mouse primary chondrocytes, and rat primary chondrocytes. We

attempted to develop mouse chondrocytes based on the study by Haseeb and Lefebvre (71). Unfortunately, we failed twice due to limited chondrocyte yield and poor proliferation. In addition, commercial mouse chondrocytes were considered too expensive. Therefore, the experiments were conducted in ATDC5 cells and rat chondrocytes. Both cell types showed similar responses to IL-1 $\beta$  and AZ. Notably, the ATDC5 cell line is derived from mouse teratocarcinoma cells, which are characterized as chondrogenic cell lines, undergoing a continuous process similar to chondrocyte differentiation; however, primary cultured chondrocytes were considered a better model and were thus selected as they appeared to be more suitable.

In conclusion, *in vitro* and *in vivo* studies demonstrated the positive effect of AZ on OA. AZ inhibited ferroptosis in chondrocytes, and mechanistically targeted the Nrf2/HO-1 pathway to inhibit the accumulation of harmful substances in chondrocyte. Furthermore, AZ attenuated articular cartilage degeneration, suggesting that targeting ferroptosis in chondrocytes may be an effective strategy for the treatment of OA. The results of the present study suggested that AZ may be an effective therapeutic candidate for OA treatment.

## Acknowledgments

The authors would like to thank the Institute of Changzhou Second People's Hospital Affiliated with Nanjing Medical University (Changzhou, China) for providing the experimental site.

## Funding

This work was supported by the Top Talent of Changzhou 'The 14th Five-Year Plan' High-Level Health Talents Training Project (grant no. 2022CZBJ078 to SN) and the Major Research Project of Changzhou Commission of Health (grant no. ZD202218 to SN).

## Availability of data and materials

The datasets used and/or analyzed during the current study are available from the corresponding author on reasonable request.

## Authors' contributions

XC, JC and SN performed experiments, obtained data, performed formal analysis and designed the study. ZZ performed experiments and analysis. XC, JC, GY and SN were involved in the methodology, conception and analysis of the study, and interpretation of data. RS and CM was involved in project administration, acquisition of data and technical assistance (synthesis of AZ). All authors read and approved the final manuscript. XC, JC, CM, GY, ZZ, RS and SN confirm the authenticity of all the raw data.

## Ethics approval and consent to participate

The present study was approved by the Jiangsu Science Standard Medical Testing Committee. Code: IACUC22-0097.

## Patient consent for publication

Not applicable.

## Competing interests

The authors declare that they have no competing interests.

## References

- Mahmoudian A, Lohmander LS, Mobasheri A, Englund M and Luyten FP: Early-stage symptomatic osteoarthritis of the knee-time for action. *Nat Rev Rheumatol* 17: 621-632, 2021.
- Glyn-Jones S, Palmer AJR, Agricola R, Price AJ, Vincent TL, Weinans H and Carr AJ: Osteoarthritis. *Lancet* 386: 376-387, 2015.
- Abramoff B and Caldera FE: Osteoarthritis. *Med Clinics North Am* 104: 293-311, 2020.
- Bijlsma JWI, Berenbaum F and Lafeber FPJG: Osteoarthritis: An update with relevance for clinical practice. *Lancet* 377: 2115-2126, 2011.
- Peng Z, Sun H, Bunpetch V, Koh Y, Wen Y, Wu D and Ouyang H: The regulation of cartilage extracellular matrix homeostasis in joint cartilage degeneration and regeneration. *Biomaterials* 268: 120555, 2021.
- Musumeci G, Castrogiovanni P, Trovato FM, Weinberg AM, Al-Wasiyah MK, Alqahtani MH and Mobasheri A: Biomarkers of chondrocyte apoptosis and autophagy in osteoarthritis. *Int J Mol Sci* 16: 20560-20575, 2015.
- Yin H, Wang Y, Sun X, Cui G, Sun Z, Chen P, Xu Y, Yuan X, Meng H, Xu W, *et al*: Functional tissue-engineered microtissue derived from cartilage extracellular matrix for articular cartilage regeneration. *Acta Biomater* 77: 127-141, 2018.
- Yang J, Hu S, Bian Y, Yao J, Wang D, Liu X, Guo Z, Zhang S and Peng L: Targeting cell death: Pyroptosis, ferroptosis, apoptosis and necroptosis in osteoarthritis. *Front Cell Dev Biol* 9: 789948, 2022.
- Bertheloot D, Latz E and Franklin BS: Necroptosis, pyroptosis and apoptosis: An intricate game of cell death. *Cell Mol Immunol* 18: 1106-1121, 2021.
- Sun K, Hou L, Guo Z, Wang G, Guo J, Xu J, Zhang X and Guo F: JNK-JUN-NCOA4 axis contributes to chondrocyte ferroptosis and aggravates osteoarthritis via ferritinophagy. *Free Radical Biol Med* 200: 87-101, 2023.
- Chen X, Kang R, Kroemer G and Tang D: Ferroptosis in infection, inflammation, and immunity. *J Exp Med* 18: e20210518, 2021.
- Jiang X, Stockwell BR and Conrad M: Ferroptosis: Mechanisms, biology and role in disease. *Nat Rev Mol Cell Biol* 22: 266-282, 2021.
- Zhou B, Liu J, Kang R, Klionsky DJ, Kroemer G and Tang D: Ferroptosis is a type of autophagy-dependent cell death. *Semin Cancer Biol* 66: 89-100, 2020.
- Tang D, Chen X, Kang R and Kroemer G: Ferroptosis: Molecular mechanisms and health implications. *Cell Res* 31: 107-125, 2021.
- Wang S, Li W, Zhang P, Wang Z, Ma X, Liu C, Vasilev K, Zhang L, Zhou X, Liu L, *et al*: Mechanical overloading induces GPX4-regulated chondrocyte ferroptosis in osteoarthritis via Piezo1 channel facilitated calcium influx. *J Adv Res* 41: 63-75, 2022.
- Friedmann Angeli JP, Schneider M, Proneth B, Tyurina YY, Tyurin VA, Hammond VJ, Herbach N, Aichler M, Walch A, Eggenhofer E, *et al*: Inactivation of the ferroptosis regulator Gpx4 triggers acute renal failure in mice. *Nat Cell Biol* 16: 1180-1191, 2014.
- Wang Y, Zheng L, Shang W, Yang Z, Li T, Liu F, Shao W, Lv L, Chai L, Qu L, *et al*: Wnt/beta-catenin signaling confers ferroptosis resistance by targeting GPX4 in gastric cancer. *Cell Death Differ* 29: 2190-2202, 2022.
- Miao Y, Chen Y, Xue F, Liu K, Zhu B, Gao J, Yin J, Zhang C and Li G: Contribution of ferroptosis and GPX4's dual functions to osteoarthritis progression. *EBioMedicine* 76: 103847, 2022.
- Wan Y, Shen K, Yu H and Fan W: Baicalein limits osteoarthritis development by inhibiting chondrocyte ferroptosis. *Free Radic Biol Med* 196: 108-120, 2023.
- He Q, Yang J, Pan Z, Zhang G, Chen B, Li S, Xiao J, Tan F, Wang Z, Chen P and Wang H: Biochanin A protects against iron overload associated knee osteoarthritis via regulating iron levels and NRF2/System xc-/GPX4 axis. *Biomed Pharmacother* 157: 113915, 2023.
- Gong Z, Wang Y, Li L, Li X, Qiu B and Hu Y: Cardamonin alleviates chondrocytes inflammation and cartilage degradation of osteoarthritis by inhibiting ferroptosis via p53 pathway. *Food Chem Toxicol* 174: 113644, 2023.
- Ma Q: Role of nrf2 in oxidative stress and toxicity. *Annu Rev Pharmacol Toxicol* 53: 401-426, 2013.
- Kerins MJ and Ooi A: The roles of NRF2 in modulating cellular iron homeostasis. *Antioxid Redox Signal* 29: 1756-1773, 2018.
- Dodson M, Castro-Portuguez R and Zhang DD: NRF2 plays a critical role in mitigating lipid peroxidation and ferroptosis. *Redox Biol* 23: 101107, 2019.
- Agyeman AS, Chaerkady R, Shaw PG, Davidson NE, Visvanathan K, Pandey A and Kensler TW: Transcriptomic and proteomic profiling of KEAP1 disrupted and sulforaphane-treated human breast epithelial cells reveals common expression profiles. *Breast Cancer Res Treat* 132: 175-187, 2012.
- Harada N, Kanayama M, Maruyama A, Yoshida A, Tazumi K, Hosoya T, Mimura J, Toki T, Maher JM, Yamamoto M and Itoh K: Nrf2 regulates ferroportin 1-mediated iron efflux and counteracts lipopolysaccharide-induced ferroportin 1 mRNA suppression in macrophages. *Arch Biochem Biophys* 508: 101-109, 2011.
- Guo Z, Lin J, Sun K, Guo J, Yao X, Wang G, Hou L, Xu J, Guo J and Guo F: Deferoxamine alleviates osteoarthritis by inhibiting chondrocyte ferroptosis and activating the Nrf2 pathway. *Front Pharmacol* 13: 791376, 2022.
- Mo Z, Xu P and Li H: Stigmasterol alleviates interleukin-1beta-induced chondrocyte injury by down-regulating sterol regulatory element binding transcription factor 2 to regulate ferroptosis. *Bioengineered* 12: 9332-9340, 2021.
- Yang J, Mo J, Dai J, Ye C, Cen W, Zheng X, Jiang L and Ye L: Cetuximab promotes RSL3-induced ferroptosis by suppressing the Nrf2/HO-1 signalling pathway in KRAS mutant colorectal cancer. *Cell Death Dis* 12: 1079, 2021.
- Cai X, Hua S, Deng J, Du Z, Zhang D, Liu Z, Khan NU, Zhou M and Chen Z: Astaxanthin activated the Nrf2/HO-1 pathway to enhance autophagy and inhibit ferroptosis, ameliorating acetaminophen-induced liver injury. *ACS Appl Mater Interfaces* 14: 42887-42903, 2022.
- Zhou X, Zhang Y, Hou M, Liu H, Yang H, Chen X, Liu T, He F and Zhu X: Melatonin prevents cartilage degradation in Early-stage osteoarthritis through activation of miR-146a/NRF2/HO-1 axis. *J Bone Miner Res* 37: 1056-1072, 2022.
- Chen M, Wen H, Zhou S, Yan X and Li H: Patchouli alcohol inhibits D-Gal induced oxidative stress and ameliorates the quality of aging cartilage via activating the Nrf2/HO-1 pathway in mice. *Oxid Med Cell Longev* 2022: 6821170, 2022.
- Xiong L, Bao H, Li S, Gu D, Li Y, Yin Q, Li W, Miao L and Liu C: Cerium oxide nanoparticles protect against chondrocytes and cartilage explants from oxidative stress via Nrf2/HO-1 pathway in temporomandibular joint osteoarthritis. *Front Bioeng Biotechnol* 11: 1076240, 2023.
- Zhang Y, Han S, Kong M, Tu Q, Zhang L and Ma X: Single-cell RNA-seq analysis identifies unique chondrocyte subsets and reveals involvement of ferroptosis in human intervertebral disc degeneration. *Osteoarthritis Cartilage* 29: 1324-1334, 2021.
- Luo P, Huang Q, Chen S, Wang Y and Dou H: Asiaticoside ameliorates osteoarthritis progression through activation of Nrf2/HO-1 and inhibition of the NF- $\kappa$ B pathway. *Int Immunopharmacol* 108: 108864, 2022.
- Witkin JM and Li X: Curcumin, an active constituent of the ancient medicinal herb *Curcuma longa* L.: Some uses and the establishment and biological basis of medical efficacy. *CNS Neurol Disord Drug Targets* 12: 487-497, 2013.
- Menon VP and Sudheer AR: Antioxidant and anti-inflammatory properties of curcumin. *Adv Exp Med Biol* 595: 105-125, 2007.
- Chaudhuri RK, Meyer T, Premi S and Brash D: Acetyl zingerone: An efficacious multifunctional ingredient for continued protection against ongoing DNA damage in melanocytes after sun exposure ends. *Int J Cosmetic Sci* 42: 36-45, 2020.
- Swindell WR, Bojanowski K and Chaudhuri RK: A Zingerone analog, acetyl zingerone, bolsters matrix synthesis, inhibits matrix metalloproteinases, and represses IL-17A target gene expression. *J Invest Dermatol* 140: 602-614.e15, 2020.
- Swindell WR, Randhawa M, Quijas G, Bojanowski K and Chaudhuri RK: Tetrahexyldecyl ascorbate (THDC) degrades rapidly under oxidative stress but can be stabilized by Acetyl zingerone to enhance collagen production and antioxidant effects. *Int J Mol Sci* 22: 8756, 2021.
- Tang Z, Zhao P, Wang H, Liu Y and Bu W: Biomedicine meets fenton chemistry. *Chem Rev* 121: 1981-2019, 2021.

42. Sun K, Luo J, Jing X, Xiang W, Guo J, Yao X, Liang S, Guo F and Xu T: Hyperoside ameliorates the progression of osteoarthritis: An in vitro and in vivo study. *Phytomedicine* 80: 153387, 2021.
43. Conlee KM, Stephens ML, Rowan AN and King LA: Carbon dioxide for euthanasia: Concerns regarding pain and distress, with special reference to mice and rats. *Lab Anim* 39: 137-161, 2005.
44. Valentim AM, Guedes SR, Pereira AM and Antunes LM: Euthanasia using gaseous agents in laboratory rodents. *Lab Anim* 50: 241-253, 2016.
45. Ahmadi-Noorbakhsh S, Mirabzadeh Ardakani E, Sadighi J, Aldavood SJ, Farajli Abbasi M, Farzad-Mohajeri S, Ghasemi A, Sharif-Paghaleh E, Hatami Z, Nikravanfar N and Shamsi Gooshki E: Guideline for the care and use of laboratory animals in Iran. *Lab Anim (NY)* 50: 303-305, 2021.
46. Danneman PJ, Stein S and Walshaw SO: Humane and practical implications of using carbon dioxide mixed with oxygen for anesthesia or euthanasia of rats. *Lab Anim Sci* 47: 376-385, 1997.
47. Tavallaei G, Lively S, Rockel JS, Ali SA, Im M, Sarda C, Mitchell GM, Rossomacha E, Nakamura S, Potla P, *et al*: Contribution of MicroRNA-27b-3p to synovial fibrotic responses in knee osteoarthritis. *Arthritis Rheumatol* 74: 1928-1942, 2022.
48. Arden NK, Perry TA, Bannuru RR, Bruyère O, Cooper C, Haugen IK, Hochberg MC, McAlindon TE, Mobasheri A and Reginster JY: Non-surgical management of knee osteoarthritis: Comparison of ESCEO and OARSI 2019 guidelines. *Nat Rev Rheumatol* 17: 59-66, 2021.
49. Hwang HS and Kim HA: Chondrocyte apoptosis in the pathogenesis of osteoarthritis. *Int J Mol Sci* 16: 26035-26054, 2015.
50. Liu Z, Chen J, Miranda AJ, Wang C, Zuscik MJ, O'Keefe RJ and Hilton MJ: A dual role for NOTCH signaling in joint cartilage maintenance and osteoarthritis. *Sci Signal* 8: ra71, 2015.
51. Lin NY, Distler A, Beyer C, Philippi-Schöbinger A, Breda S, Dees C, Stock M, Tomcik M, Niemeier A, Dell'Accio F, *et al*: Inhibition of Notch1 promotes hedgehog signalling in a HES1-dependent manner in chondrocytes and exacerbates experimental osteoarthritis. *Ann Rheum Dis* 75: 2037-2044, 2016.
52. Narayana Y and Balaji KN: NOTCH1 up-regulation and signaling involved in Mycobacterium bovis BCG-induced SOCS3 expression in macrophages. *J Biol Chem* 283: 12501-12511, 2008.
53. Linkermann A, Skouta R, Himmerkus N, Mulay SR, Dewitz C, De Zen F, Prokai A, Zuchtriegel G, Krombach F, Welz PS, *et al*: Synchronized renal tubular cell death involves ferroptosis. *Proc Natl Acad Sci USA* 111: 16836-16841, 2014.
54. Li Y, Feng D, Wang Z, Zhao Y, Sun R, Tian D, Liu D, Zhang F, Ning S, Yao J and Tian X: Ischemia-induced ACSL4 activation contributes to ferroptosis-mediated tissue injury in intestinal ischemia/reperfusion. *Cell Death Differ* 26: 2284-2299, 2019.
55. Wang Y, Yan S, Liu X, Deng F, Wang P, Yang L, Hu L, Huang K and He J: PRMT4 promotes ferroptosis to aggravate doxorubicin-induced cardiomyopathy via inhibition of the Nrf2/GPX4 pathway. *Cell Death Differ* 29: 1982-1995, 2022.
56. Zi Y, Wang X, Zi Y, Yu H, Lan Y, Fan Y, Ren C, Liao K and Chen H: Cigarette smoke induces the ROS accumulation and iNOS activation through deactivation of Nrf-2/SIRT3 axis to mediate the human bronchial epithelium ferroptosis. *Free Radic Biol Med* 200: 73-86, 2023.
57. Kuang L, Wu J, Su N, Qi H, Chen H, Zhou S, Xiong Y, Du X, Tan Q, Yang J, *et al*: FGFR3 deficiency enhances CXCL12-dependent chemotaxis of macrophages via upregulating CXCR7 and aggravates joint destruction in mice. *Ann Rheum Dis* 79: 112-122, 2020.
58. Hosaka Y, Saito T, Sugita S, Hikata T, Kobayashi H, Fukai A, Taniguchi Y, Hirata M, Akiyama H, Chung UI and Kawaguchi H: Notch signaling in chondrocytes modulates endochondral ossification and osteoarthritis development. *Proc Natl Acad Sci USA* 110: 1875-1880, 2013.
59. Artavanis-Tsakonas S, Rand MD and Lake RJ: Notch signaling: Cell fate control and signal integration in development. *Science* 284: 770-776, 1999.
60. Dixon SJ, Lemberg KM, Lamprecht MR, Skouta R, Zaitsev EM, Gleason CE, Patel DN, Bauer AJ, Cantley AM, Yang WS, *et al*: Ferroptosis: An iron-dependent form of nonapoptotic cell death. *Cell* 149: 1060-1072, 2012.
61. Wang W, Jing X, Du T, Ren J, Liu X, Chen F, Shao Y, Sun S, Yang G and Cui X: Iron overload promotes intervertebral disc degeneration via inducing oxidative stress and ferroptosis in endplate chondrocytes. *Free Radical Biol Med* 190: 234-246, 2022.
62. Xiang Q, Zhao Y, Lin J, Jiang S and Li W: The Nrf2 antioxidant defense system in intervertebral disc degeneration: Molecular insights. *Exp Mol Med* 54: 1067-1075, 2022.
63. Torrente L and DeNicola GM: Targeting NRF2 and its downstream processes: Opportunities and challenges. *Ann Rev Pharmacol Toxicol* 62: 279-300, 2022.
64. Li J, Lu K, Sun F, Tan S, Zhang X, Sheng W, Hao W, Liu M, Lv W and Han W: Panaxydol attenuates ferroptosis against LPS-induced acute lung injury in mice by Keap1-Nrf2/HO-1 pathway. *J Transl Med* 19: 96, 2021.
65. Ma H, Wang X, Zhang W, Li H, Zhao W, Sun J and Yang M: Melatonin suppresses ferroptosis induced by high glucose via activation of the Nrf2/HO-1 signaling pathway in type 2 diabetic osteoporosis. *Oxid Med Cell Longev* 2020: 9067610, 2020.
66. Wu S, Zhu J, Wu G, Hu Z, Ying P, Bao Z, Ding Z and Tan X: 6-Gingerol alleviates ferroptosis and inflammation of diabetic cardiomyopathy via the Nrf2/HO-1 pathway. *Oxid Med Cell Longev* 2022: 3027514, 2022.
67. Li S, Zhou C, Zhu Y, Chao Z, Sheng Z, Zhang Y and Zhao Y: Ferrostatin-1 alleviates angiotensin II (Ang II)-induced inflammation and ferroptosis in astrocytes. *Int Immunopharmacol* 90: 107179, 2021.
68. Yang Y, Cai X, Yang J, Sun X, Hu C, Yan Z, Xu X, Lu W, Wang X and Cao P: Chemoprevention of dietary digitoflavone on colitis-associated colon tumorigenesis through inducing Nrf2 signaling pathway and inhibition of inflammation. *Mol Cancer* 13: 48, 2014.
69. Hourihan JM, Moronetti Mazzeo LE, Fernández-Cárdenas LP and Blackwell TK: Cysteine sulfonylation directs IRE-1 to activate the SKN-1/Nrf2 antioxidant response. *Mol Cell* 63: 553-566, 2016.
70. Liu Z, Lang Y, Li L, Liang Z, Deng Y, Fang R and Meng Q: Effect of emodin on chondrocyte viability in an *in vitro* model of osteoarthritis. *Exp Ther Med* 16: 5384-5389, 2018.
71. Haseeb A and Lefebvre V: Isolation of Mouse Growth Plate and Articular Chondrocytes for Primary Cultures. *Methods Mol Biol* 2245: 39-51, 2021.



Copyright © 2023 Chen et al. This work is licensed under a Creative Commons Attribution-NonCommercial-NoDerivatives 4.0 International (CC BY-NC-ND 4.0) License.